nature physics

LETTERS

PUBLISHED ONLINE: 21 SEPTEMBER 2015 | DOI: 10.1038/NPHYS3470

Three-stage decoherence dynamics of an electron spin qubit in an optically active quantum dot

Alexander Bechtold[1], Dominik Rauch[1], Fuxiang Li[2,3], Tobias Simmet[1], Per-Lennart Ardelt[1], Armin Regler[1,4], Kai Müller[1,4], Nikolai A. Sinitsyn[3] and Jonathan J. Finley[1]*

The control of solid-state qubits requires a detailed understanding of the decoherence mechanisms. Despite considerable progress in uncovering the qubit dynamics in strong magnetic fields[1–4], decoherence at very low magnetic fields remains puzzling, and the role of quadrupole coupling of nuclear spins is poorly understood. For spin qubits in semiconductor quantum dots, phenomenological models of decoherence include two basic types of spin relaxation[5–7]: fast dephasing due to static but randomly distributed hyperfine fields (∼2 ns)[8–11] and a much slower process (>1 μs) of irreversible monotonic relaxation due either to nuclear spin co-flips or other complex many-body interaction effects[12]. Here we show that this is an oversimplification; the spin qubit relaxation is determined by three rather than two distinct stages. The additional stage corresponds to the effect of coherent precession processes that occur in the nuclear spin bath itself, leading to a relatively fast but incomplete non-monotonic relaxation at intermediate timescales (∼750 ns).

A coupling of the central spin to the nuclear spin bath gives rise to an effective magnetic field, the Overhauser field[5,6,13,14], around which the central spin precesses at nanosecond timescales[3,15–17]. Numerous theoretical studies predicted that in the absence of external magnetic fields the coherent character of this precession leads to a characteristic dip in the central spin relaxation—that is, the spin polarization reaches a minimum during a few nanoseconds, from which it recovers before reaching a nearly steady level at 1/3 of the initial polarization[5,18]. The fate of the remaining polarization has been the subject of considerable debate. Early studies predicted, for example, that the randomness of hyperfine couplings can lead to an intermediate stage of a qubit relaxation that has qualitatively similar features to a dephasing stage[5]. However, subsequent theoretical[6,12,19,20] and numerical studies[7] showed that the randomness of parameters leads only to a slow, $\sim 1/\log(t)$, and incomplete monotonic relaxation. Weak dipole interactions between nuclear spins were predicted to lead to a complete relaxation during millisecond timescales[2,5], but even this theory was challenged by the observation of hour-long nuclear spin relaxation, which suggested the importance of quadrupole couplings[21]. Unfortunately, until now it has been impossible to test many such predictions experimentally, in particular, to observe the predicted dip in the qubit relaxation dynamics and explore phenomena occurring at much longer timescales. Here, we apply novel experimental techniques that not only clearly resolve the precession dip in the spin qubit relaxation but also provide new insights into the time dependence of the central spin qubit during up to four orders of magnitude longer timescales. Hereby, we make use of a spin storage device[22] in which a single electron spin can be optically prepared in the quantum dot (QD) over picosecond timescales with near perfect fidelity[23] and stored over milliseconds[24]. After a well-defined storage time we directly measure the electron spin projection along the optical axis and show that the electron spin qubit exhibits three distinct stages of relaxation. The first stage arises from a spin evolution in the randomly oriented quasi-static Overhauser field as a consequence of hyperfine interaction (Fig. 1a, γ_{HF}) inducing an inhomogeneous dephasing over the initial few nanoseconds. This is followed by an unexpected stage of the central spin relaxation, namely the appearance of a second dip in the relaxation curve after several hundred nanoseconds. We show that this feature reflects coherent dynamic processes in the nuclear spin bath itself induced by quadrupolar coupling (Fig. 1a, γ_{Q}) of nuclear spins I to the strain-induced electric field gradients ∇E (refs 25–27). Eventually, the combined effect of quadrupolar coherent nuclear spin dynamics and incoherent co-flips of nuclear spins with the central spin, and possibly other interactions, induce the third stage with monotonic relaxation that occurs over microsecond timescales and low magnetic fields.

The electron spin qubit studied in this work is confined in a single self-assembled InGaAs QD incorporated in the intrinsic region of a Schottky photodiode structure next to an AlGaAs tunnel barrier (Methods). As illustrated in the schematic band diagram in Fig. 1b, such an asymmetric tunnel barrier design facilitates control of the electron (τ_{e}) and hole (τ_{h}) tunnelling time by switching the electric field inside the device. Such a control enables different modes of operation (Fig. 1c): discharging the QD at high electric fields (Reset), optical electron spin initialization realized by applying a single optical picosecond polarized laser pulse (Pump), spin-to-charge conversion (Probe) after a spin storage time T_{store}, and charge read-out (Read) by measuring the photoluminescence (PL) yield obtained by cycling the optical $e^- \rightarrow X_{3/2}^{-1}$ transition[28,29] (for detailed information see Supplementary Sections 1 and 2). Figure 1d compares typical PL signatures of the electron spin read-out scheme for applied magnetic fields of $|\mathbf{B}_z| = 80$ mT and 0 mT at a fixed storage time of 2.8 ns. To measure the spin polarization $\langle S_z \rangle$ we perform two different measurement sequences; a reset–pump–read cycle (black points in Fig. 1d) to obtain the PL intensity as a reference when only one electron is present in the QD and a reset–pump–probe–read cycle (red points in Fig. 1d) from which we deduce the average charge occupation of the QD (1e or 2e) by comparing the PL intensities of the $X_{3/2}^{-1}$ ground state recombination ($I_{1\mathrm{e}}$ or $I_{2\mathrm{e}}$). The degree of spin polarization is then given by

[1]Walter Schottky Institut, Technische Universität München, 85748 Garching, Germany. [2]Center for Nonlinear Studies, Los Alamos National Laboratory, Los Alamos, New Mexico 87545, USA. [3]Theoretical Division, Los Alamos National Laboratory, Los Alamos, New Mexico 87545, USA. [4]E. L. Ginzton Laboratory, Stanford University, Stanford, California 94305, USA. *e-mail: jonathan.finley@wsi.tum.de

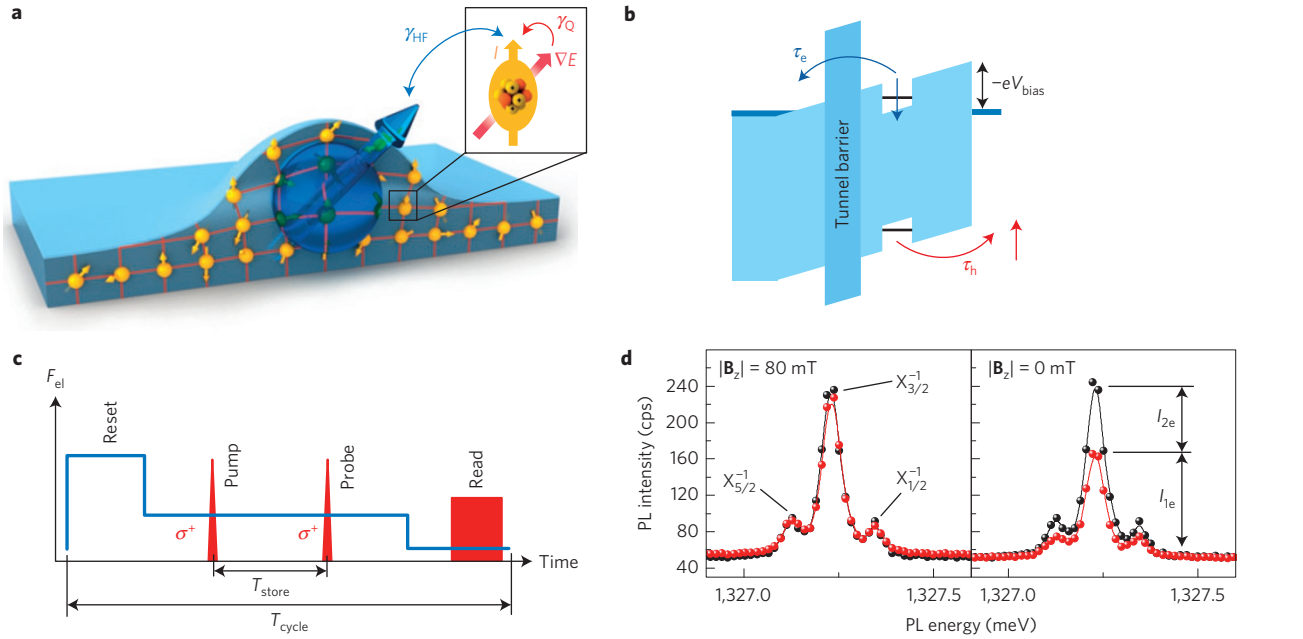

Figure 1 | Single electron spin preparation, storage and read-out. a, Illustration of the hyperfine interaction (γ_{HF}) between an electron spin (blue arrow) and the nuclear spins (yellow arrows), and quadrupolar interaction (γ_Q) between the strain-induced electric field gradient ∇E and the nuclear spins I. **b**, Schematic representation of the band profile of the spin memory device. **c**, Representation of the applied electric field and optical pulse sequence as a function of time. The measurement cycle consists of four phases: discharging the QD (Reset), electron spin preparation (Pump), spin-to-charge conversion for spin measurement (Probe) and charge read-out (Read). **d**, Photoluminescence (PL) signature of the electron spin read-out for storage times of $T_{store} = 2.8$ ns. The $X^{-1}_{3/2}$ PL intensity reflects the charge state of the QD, 1e or 2e, by comparison of the luminescence yield obtained with (red points) and without (black points) the application of a probe pulse.

$\langle S_z \rangle = (I_{1e} - I_{2e})/(I_{1e} + I_{2e})$. As can be seen in Fig. 1d, on reducing the magnetic field, the probability of finding the dot charged with 2e rises ($I_{2e} > 0$), indicating that electron spin relaxation has occurred and consequently we find $\langle S_z \rangle < 1$.

The temporal evolution of $\langle S_z \rangle$ at zero external magnetic field is presented in Fig. 2a. Over the initial 20 ns the average electron spin polarization exhibits a strong decay due to precession of the initial electron spin $\mathbf{S}_0$ around a frozen Overhauser field $\mathbf{B}_n$ (as schematically depicted in Fig. 2b, top). At these short timescales the Overhauser field experienced by the electron can be treated as being quasi-static but evolving between measurement cycles during the few-second integration time of our experiment. The magnitude and direction of $\mathbf{B}_n$ are described by a Gaussian distribution function $W(\mathbf{B}_n) \propto \exp(-\mathbf{B}_n^2/2\sigma_n^2)$, with σ_n being the dispersion of the Overhauser field[5]. As a consequence of the field fluctuations with dispersion σ_n, the electron Larmor precession around the Overhauser field, averaged over many precession frequencies, leads to a characteristic dip in $\langle S_z \rangle$ reflecting the inhomogeneous dephasing time $T_2^* = 2$ ns. The initial degree of spin polarization after the electron has been initialized amounts to $S_0 = 85\%$. This observation may be indicative of a weak magnetic interaction between the tunnelling hole and the stored electron during the partial exciton ionization. This conclusion is supported by the fact that S_0 returns to $\sim 100\%$ when a weak static magnetic field ($|\mathbf{B}_z| > 50$ mT) is applied.

In the second phase of spin relaxation observed in Fig. 2a, which takes place from 20 ns to 1 µs, the degree of spin polarization is further reduced from $\langle S_z \rangle \sim 1/3$ to a small non-vanishing value $\langle S_z \rangle \sim 1/9$. After this stage, only a small monotonic relaxation is observed up to 10 µs. In order to quantify the experimental data in Fig. 2a, we developed a semi-classical model in which the nuclear spins precess around the random static quadrupolar fields combined with a time-dependent hyperfine field of the central spin (Methods). The quadrupolar coupling of an ith nuclear spin is characterized by the direction of the coupling axis $\mathbf{n}^i$ and by the size of the energy level splitting γ_Q^i along this quantization axis. In a self-assembled quantum dot, electric field gradients have a broad distribution of their direction and magnitude. We modelled them by assuming that the directions of quadrupolar coupling axes are uniformly distributed and the characteristic level splittings have Gaussian distribution throughout the spin bath: $W(\gamma_Q^i) \propto \exp(-(\gamma_Q^i)^2/2\sigma_Q^2)$, with σ_Q being the single parameter that characterizes the distribution of the quadrupolar coupling strengths in the spin bath.

The red line in Fig. 2a shows the prediction of this model obtained in the limit that disregards the impact of the central spin on the nuclear spin dynamics. Even in this limit the model correctly captures the appearance of both relaxation dips. The position of the first dip is determined by the Overhauser field distribution $\sigma_n = 10.3$ mT. Our semi-classical model explains the second dip as being due to coherent precession of nuclear spins around the quadrupolar axes. The time-correlator of the Overhauser field produced by all precessing nuclear spins then has a dip at a characteristic precession frequency and saturates at a non-zero value. Throughout this regime the central spin follows the Overhauser field adiabatically, and thus its relaxation directly reflects the shape of the Overhauser field correlator. The position of the second dip is then determined only by the quadrupolar coupling strength, $T_Q = \sqrt{3}/\sigma_Q$, resulting in a value $\sigma_Q = 2.3\,\mu s^{-1}$, and is in good agreement with the quadrupole splitting of $\sim 1.4\,\mu s^{-1}$ obtained in ref. 26 using optically detected nuclear magnetic resonance (ODNMR) spectroscopy at large magnetic fields. Finally, to capture the many-body co-flip effects beyond perturbative limits within the nuclear spin bath, we performed numerical simulations of our semi-classical model including up to $N = 50{,}000$ spins. The result of these simulations at $\sigma_Q = 2\langle\gamma_{HF}\rangle$ is presented in the inset of Fig. 2a. It demonstrates that complex many-body interactions, such as spin co-flips, do not remove either of the relaxation dips provided the quadrupolar coupling strength exceeds the hyperfine coupling

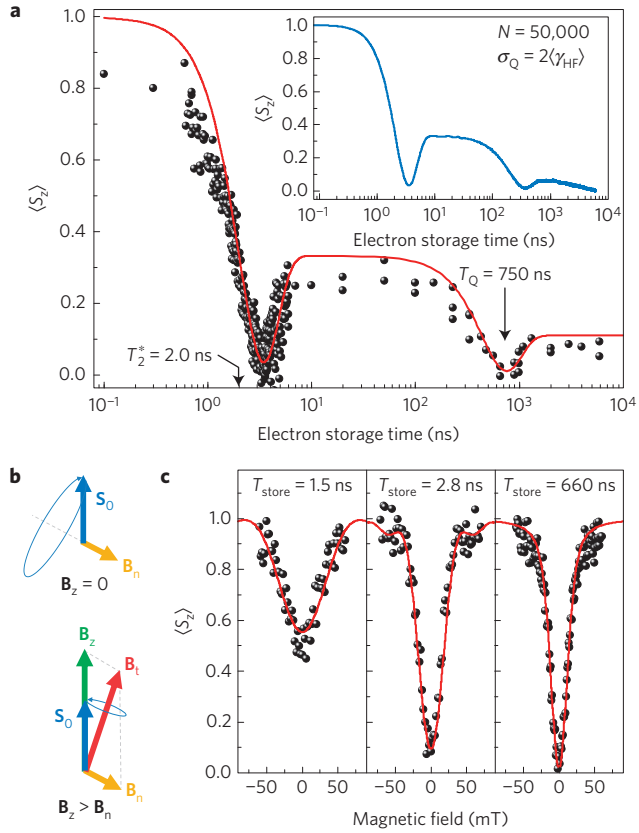

Figure 2 | Dynamics of the electron spin relaxation. a, Experimental data reveal a fast inhomogeneous electron spin dephasing T_2^*. The quadrupolar coupling of nuclear spins induces oscillatory fluctuations of the Overhauser field at T_Q, which further reduces $\langle S_z\rangle$. The red line compares experimental results with analytical predictions based on the semi-classical model (Supplementary Equations 7 and 14). The inset presents results of more rigorous numerical simulations based on the theoretical model of central spin decoherence by a nuclear spin bath (Methods). The long relaxation tail at longer times (>1 μs) is due to combined effects of hyperfine and quadrupolar coupling. **b**, Illustration of electron spin evolution with an initial spin $\mathbf{S}_0$ in a total magnetic field $\mathbf{B}_t$. **c**, Evolution of the electron spin in weak out-of-plane magnetic fields. The width of the dip characterizes the variance of the Overhauser field distribution. A semi-classical model (red line) was used to simulate the experimental data (Supplementary Equations 6 and 15).

$\sigma_Q > \langle\gamma_{HF}\rangle$, (see Supplementary Fig. 5 and associated discussion). Moreover, numerical results show that quadrupole coupling enhances the remaining irreversible relaxation via co-flips of nuclear spins with the central spin. Hence, it can be responsible for the irreversible third stage of central spin relaxation at zero external fields.

To obtain the Overhauser field dispersion experimentally we performed magnetic-field-dependent measurements of $\langle S_z\rangle$, presented in Fig. 2c. The data clearly show that $\langle S_z\rangle$ resembles a dip at low magnetic fields, which can be explained as follows: in the presence of the Overhauser field $\mathbf{B}_n$ the electron spin precesses about the total field $\mathbf{B}_t = \mathbf{B}_n + \mathbf{B}_z$, as schematically depicted in Fig. 2b (bottom). At strong external magnetic fields ($|\mathbf{B}_z| \gg |\mathbf{B}_n|$) the total magnetic field $\mathbf{B}_t$ is effectively directed along $\mathbf{B}_z$ and the Zeeman interaction of the electron spin with the magnetic field is larger than the interaction with the Overhauser field. As a consequence, the electron spin relaxation is suppressed by an application of $\mathbf{B}_z$, resulting in $\langle S_z\rangle \simeq 1$, as can be seen in Fig. 2c for $|\mathbf{B}_z| > 50$ mT. By fitting our data using a semi-classical model (red solid line in Fig. 2c) we extract a dispersion of $\sigma_n = 10.5$ mT that remains approximately constant at the storage times explored.

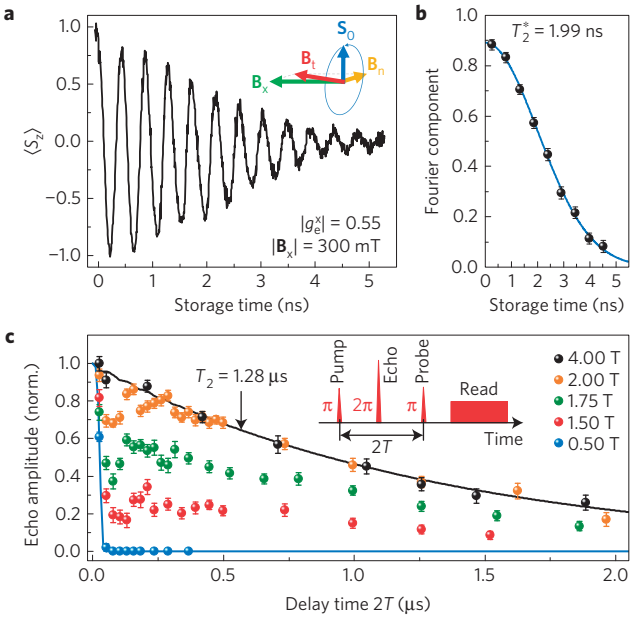

Figure 3 | Evolution of the electron spin in an in-plane magnetic field. **a**, Free-induction decay of the electron spin qubit. The Larmor oscillations are damped owing to fluctuations of the Overhauser field. **b**, The Fourier component of the Larmor oscillations decays according to a Gaussian function, revealing the spin dephasing time T_2^*. Error bars represent one-standard-deviation confidence intervals from a sinusoidal fit to the data over two Larmor periods. **c**, Echo signal as a function of the total evolution time at different magnetic fields. The fit of the data at high (black) and low (blue) magnetic fields are obtained using a theoretical model which is described in the Supplementary Section 4. Error bars represent one-standard-deviation confidence intervals estimated by taking multiple measurements of the same delay curve.

In addition to the out-of-plane magnetic field measurements, where the electron spin is prepared in a spin-eigenstate, we show in Fig. 3a spin-precession measurements in a fixed in-plane magnetic field. Here, the electron spin, prepared along the optical z-axis, precesses with the Larmor frequency ($|g_e| = 0.55$) around $\mathbf{B}_t$, mainly directed along $\mathbf{B}_x$. Again, owing to fluctuations of the Overhauser field, the electron spin experiences a dephasing leading to damped oscillations in the evolution of $\langle S_z\rangle$. In Fig. 3b we analysed the Fourier component of the Larmor oscillations, revealing a Gaussian envelope function indicating the Gaussian-like distribution of the Overhauser field. The variance of the fit in Fig. 3b reflects the inhomogeneous dephasing time $T_2^* = 1.99 \pm 0.03$ ns, which is in perfect agreement with the value obtained in Fig. 2a, and is not affected by an application of an external magnetic field. The dephasing time and the Overhauser field dispersion are connected via $T_2^* = \hbar/g_e\mu_B\sigma_n$. Using $g_e = 0.55$ we obtain $\sigma_n = 10.3$ mT.

To remove the inhomogeneous dephasing T_2^* and investigate T_2 decoherence, we extended our pulse sequence by an additional optical (Echo) pulse which allows the implementation of spin-echo pulse sequences[3,17]. The result is shown in Fig. 3c. At strong magnetic fields ($|\mathbf{B}_x| = 4$ T) the nuclear Zeeman splitting exceeds the quadrupolar splitting of 2.3 μs^{-1} considerably, which effectively suppresses the dephasing effect of quadrupole coupling and, in contrast to the $|\mathbf{B}_x| = 0$ T measurements discussed above, a transition to a mono-exponential decay is observed. From the fit we obtain a decoherence time of $T_2 = 1.28 \pm 0.07$ μs. Such mono-exponential decay at very high magnetic fields is notable and contrary to theoretical predictions[2] and experimental observations in gate-defined QDs (ref. 3), where the decoherence could clearly be attributed to spectral diffusion arising from dipolar interactions between nuclei with much longer coherence times. However, such a

mono-exponential behaviour was also observed in earlier studies of spin-echo decay on optically active QDs (ref. 17). The exact origin of such a decoherence in self-assembled QDs is so far not fully understood and therefore still under debate. A possible source of this behaviour could arise from effects of charge-noise-induced spectral diffusion. Our theoretical model based only on quadrupole and hyperfine interactions does not explain this relaxation at large fields. However, it does explain the qualitative behaviour of the spin-echo signal at lower field. In particular, on reducing the magnetic field to the range $|\mathbf{B}_x| \sim \sqrt{\hbar g_e \sigma_n \sigma_Q / g_N^2 \mu_B} \approx 1.5\,\mathrm{T}$, where g_N is the nuclear spin g-factor, our model predicts that the quadrupolar coupling should lead to an oscillatory behaviour of the spin-echo signal (see Supplementary Section 4). Indeed, at such values of the external field we observe such oscillations. At even lower external fields, the model predicts a phase with relatively fast monotonic spin-echo relaxation as $\exp(-aT^4)$, with $a \sim 1/(T_2^* T_Q)^2$, again in excellent qualitative agreement with our experimental observations.

Our findings have major implications for extending the coherence time evolution of electron spin qubits at low magnetic fields. Whereas the inhomogeneous dephasing time T_2^* can be reversed by the application of spin-echo methods, the strong back-action of quadrupolar couplings in the spin bath demonstrates the necessity of the development of strain-engineered QD structures for extended coherence times T_2, which may also help pave the way towards creating useful semiconductor-based spin qubits that can be incorporated into quantum information devices.

Methods

Methods and any associated references are available in the online version of the paper.

Received 7 May 2015; accepted 11 August 2015; published online 21 September 2015

References

1. Cywinski, L., Witzel, W. M. & Das Sarma, S. Electron spin dephasing due to hyperfine interactions with a nuclear spin bath. *Phys. Rev. Lett.* **102,** 057601 (2009).
2. Witzel, W. M. & Das Sarma, S. Quantum theory for electron spin decoherence induced by nuclear spin dynamics in semiconductor quantum computer architectures: Spectral diffusion of localized electron spins in the nuclear solid-state environment. *Phys. Rev. B* **74,** 035322 (2006).
3. Bluhm, H. *et al.* Dephasing time of GaAs electron-spin qubits coupled to a nuclear bath exceeding 200 μs. *Nature Phys.* **7,** 109–113 (2010).
4. Zhao, N., Ho, S.-W. & Liu, R.-B. Decoherence and dynamical decoupling control of nitrogen vacancy center electron spins in nuclear spin baths. *Phys. Rev. B* **85,** 115303 (2012).
5. Merkulov, I. A., Efros, A. L. & Rosen, M. Electron spin relaxation by nuclei in semiconductor quantum dots. *Phys. Rev. B* **65,** 205309 (2002).
6. Khaetskii, A. V., Loss, D. & Glazman, L. Electron spin decoherence in quantum dots due to interaction with nuclei. *Phys. Rev. Lett.* **88,** 186802 (2002).
7. Al-Hassanieh, K. A., Dobrovitski, V. V., Dagotto, E. & Harmon, B. N. Numerical modeling of the central spin problem using the spin-coherent-state P representation. *Phys. Rev. Lett.* **97,** 037204 (2006).
8. Faribault, A. & Schuricht, D. Spin decoherence due to a randomly fluctuating spin bath. *Phys. Rev. B* **88,** 085323 (2013).
9. Braun, P.-F. *et al.* Direct observation of the electron spin relaxation induced by nuclei in quantum dots. *Phys. Rev. Lett.* **94,** 116601 (2005).
10. Dou, X. M., Sun, B. Q., Jiang, D. S., Ni, H. Q. & Niu, Z. C. Electron spin relaxation in a single InAs quantum dot measured by tunable nuclear spins. *Phys. Rev. B* **84,** 033302 (2011).
11. Johnson, A. C. *et al.* Triplet–singlet spin relaxation via nuclei in a double quantum dot. *Nature* **435,** 925–928 (2005).
12. Erlingsson, S. & Nazarov, Y. Evolution of localized electron spin in a nuclear spin environment. *Phys. Rev. B* **70,** 205327 (2004).
13. Testelin, C., Bernardot, F., Eble, B. & Chamarro, M. Hole-spin dephasing time associated with hyperfine interaction in quantum dots. *Phys. Rev. B* **79,** 195440 (2009).
14. Abragam, A. *The Principles of Nuclear Magnetism* (Clarendon, 1973).
15. Koppens, F. H. L., Nowack, K. C. & Vandersypen, L. M. K. Spin echo of a single electron spin in a quantum dot. *Phys. Rev. Lett.* **100,** 236802 (2008).
16. Petta, J. R. *et al.* Coherent manipulation of coupled electron spins in semiconductor quantum dots. *Science* **309,** 2180–2184 (2005).
17. Press, D. *et al.* Ultrafast optical spin echo in a single quantum dot. *Nature Photon.* **4,** 367–370 (2010).
18. Zhang, W., Dobrovitski, V. V., Al-Hassanieh, K. A., Dagotto, E. & Harmon, B. N. Hyperfine interaction induced decoherence of electron spins in quantum dots. *Phys. Rev. B* **74,** 205313 (2006).
19. Hackmann, J. & Anders, F. B. Spin noise in the anisotropic central spin model. *Phys. Rev. B* **89,** 045317 (2014).
20. Chen, G., Bergman, D. L. & Balents, L. Semiclassical dynamics and long-time asymptotics of the central-spin problem in a quantum dot. *Phys. Rev. B* **76,** 045312 (2007).
21. Maletinsky, P., Kroner, M. & Imamoglu, A. Breakdown of the nuclear-spin-temperature approach in quantum-dot demagnetization experiments. *Nature Phys.* **5,** 407–411 (2009).
22. Kroutvar, M. *et al.* Optically programmable electron spin memory using semiconductor quantum dots. *Nature* **432,** 81–84 (2004).
23. Müller, K. *et al.* All optical quantum control of a spin-quantum state and ultrafast transduction into an electric current. *Sci. Rep.* **3,** 1906 (2013).
24. Heiss, D. *et al.* Selective optical charge generation, storage, and readout in a single self-assembled quantum dot. *Appl. Phys. Lett.* **94,** 072108 (2009).
25. Bulutay, C. Quadrupolar spectra of nuclear spins in strained $In_xGa_{1-x}As$ quantum dots. *Phys. Rev. B* **85,** 115313 (2012).
26. Chekhovich, E. A. *et al.* Structural analysis of strained quantum dots using nuclear magnetic resonance. *Nature Nanotech.* **7,** 646–650 (2012).
27. Chekhovich, E. A., Hopkinson, M., Skolnick, M. S. & Tartakovskii, A. I. Suppression of nuclear spin bath fluctuations in self-assembled quantum dots induced by inhomogeneous strain. *Nature Commun.* **6,** 6348 (2015).
28. Jovanov, V., Kapfinger, S., Bichler, M., Abstreiter, G. & Finley, J. J. Direct observation of metastable hot trions in an individual quantum dot. *Phys. Rev. B* **84,** 235321 (2011).
29. Akimov, I. A., Hundt, A., Flissikowski, T. & Henneberger, F. Fine structure of the trion triplet state in a single self-assembled semiconductor quantum dot. *Appl. Phys. Lett.* **81,** 4730–4732 (2002).

Acknowledgements

We are very grateful to L. Cywinski for most useful and enlightening discussions. Furthermore, we gratefully acknowledge financial support from the Deutsche Forschungs Gemeinschaft via SFB-631, and the Nanosystems Initiative Munich, the EU via S3 Nano, and BaCaTeC. K.M. acknowledges financial support from the Alexander von Humboldt Foundation and the ARO (Grant W911NF-13-1-0309). Work at LANL was supported by the US Department of Energy, Contract No. DE-AC52-06NA25396, and the LDRD program at LANL.

Author contributions

A.B. and D.R. performed the experiments and data analysis with T.S. and P.-L.A. providing expertise. A.R. carried out the sample processing. F.L. and N.A.S. performed the theoretical calculations. A.B., P.-L.A., K.M., F.L., N.A.S. and J.J.F. wrote the article. A.B., K.M. and J.J.F. conceived, led and managed the project.

Additional information

Supplementary information is available in the online version of the paper. Reprints and permissions information is available online at www.nature.com/reprints. Correspondence and requests for materials should be addressed to J.J.F.

Competing financial interests

The authors declare no competing financial interests.

Methods

Sample. The sample studied consists of a low-density ($<5\,\mu m^{-2}$) layer of nominally $In_{0.5}Ga_{0.5}As$–GaAs self-assembled QDs incorporated into the $d = 140$ nm-thick intrinsic region of a Schottky photodiode structure. A opaque gold contact with micrometre-sized apertures was fabricated on top of the device to optically isolate single dots. An asymmetric $Al_{0.3}Ga_{0.7}As$ tunnel barrier with a thickness of 20 nm was grown immediately below the QDs, preventing electron tunnelling after exciton generation.

Theoretical model and numerical approximations. The minimal Hamiltonian of the central spin interacting with a nuclear spin bath with quadrupole couplings is given by

$$\hat{H} = \sum_{i=1}^{N} \left(\gamma_{\mathrm{H}}^{i} \hat{\mathbf{I}}^{i} \cdot \hat{\mathbf{S}} + g_{\mathrm{e}} \mu_{\mathrm{e}} \mathbf{B}_{\mathrm{ex}} \cdot \hat{\mathbf{S}} + g_{\mathrm{n}} \mu_{\mathrm{n}} \mathbf{B}_{\mathrm{ex}} \cdot \hat{\mathbf{I}}^{i} + \frac{\gamma_{\mathrm{q}}^{i}}{2} (\hat{\mathbf{I}}^{i} \cdot \mathbf{n}^{i})^{2} \right) \quad (1)$$

where $\hat{\mathbf{S}}$ and $\hat{\mathbf{I}}^{i}$ are operators for, respectively, the central spin and the ith nuclear spin; γ_{H}^{i} and γ_{q}^{i} are the strengths of, respectively, the hyperfine and the quadrupole couplings of ith nuclear spin, $I^{i} > 1/2$ are the sizes of the nuclear spins, for example, $I = 3/2$ for Ga and $I = 9/2$ for most abundant In isotopes; $\mathbf{B}_{\mathrm{ex}}$ is the external magnetic field; $\mathbf{n}^{i}$ is the unit vector along the direction of the quadrupole coupling anisotropy, which generally has a broad distribution inside a self-assembled quantum dot. The analytical and even numerical treatment of evolution with equation (1) would be too complex to achieve for a realistic number of nuclear spins $N \sim 10^{5}$. To obtain such estimates, we used an observation made in ref. 30 that essential effects of the quadrupole coupling in (1) are captured by a much simpler model of a spin bath with spins-1/2 only:

$$\hat{H} = \mathbf{B} \cdot \hat{\mathbf{S}} + \sum_{i=1}^{N} \gamma_{\mathrm{H}}^{i} \hat{\mathbf{S}} \cdot \hat{\mathbf{s}}^{i} + \gamma_{\mathrm{Q}}^{i} (\hat{\mathbf{s}}^{i} \cdot \mathbf{n}^{i}) + \mathbf{b} \cdot \hat{\mathbf{s}}^{i}$$

with $\mathbf{B} = g_{\mathrm{e}} \mu_{\mathrm{e}} \mathbf{B}_{\mathrm{ex}}$ and $\mathbf{b} = g_{\mathrm{N}} \mu_{\mathrm{N}} \mathbf{B}_{\mathrm{ex}}$ the effective Zeeman fields acting on, respectively, electron and nuclear spins. The spin-1/2 operator $\hat{\mathbf{s}}^{i}$ stands for the ith nuclear spin. The quadrupole coupling is mimicked here by introducing random static magnetic fields acting on nuclear spins with the same distribution of $\mathbf{n}^{i}$ as in (1)—that is, the vector $\mathbf{n}^{i}$ points in a random direction, different for each nuclear spin. Parameter γ_{Q}^{i} is connected to γ_{q}^{i} as $\gamma_{\mathrm{Q}}^{i} \sim \gamma_{\mathrm{q}}^{i} I/2$. It is the characteristic nearest energy level splitting of a nuclear spin due to the quadrupole coupling.

References

30. Sinitsyn, N. A., Li, Y., Crooker, S. A., Saxena, A. & Smith, D. L. Role of nuclear quadrupole coupling on decoherence and relaxation of central spins in quantum dots. *Phys. Rev. Lett.* **109,** 166605 (2012).